Inorganic Chemistry

Article

pubs.acs.org/IC

# Synthesis, Steady-State, and Femtosecond Transient Absorption Studies of Resorcinol Bound Ruthenium(II)- and Osmium(II)-polypyridyl Complexes on Nano-$TiO_2$ Surface in Water

Tanmay Banerjee,[†] Sreejith Kaniyankandy,[‡] Amitava Das,*[,†] and Hirendra Nath Ghosh*[,‡]

[†]Central Salt and Marine Chemicals Research Institute, Bhavnagar 364002, India

[‡]Radiation and Photochemistry Division, Bhabha Atomic Research Centre, Mumbai 400085, India

Supporting Information

**ABSTRACT:** The synthesis of two new ruthenium(II)- and osmium(II)-polypyridyl complexes **3** and **4**, respectively, with resorcinol as the enediol anchoring moiety, is described. Steady-state photochemical and electrochemical studies of the two sensitizer dyes confirm strong binding of the dyes to $TiO_2$ in water. Femtosecond transient absorption studies have been carried out on the dye−$TiO_2$ systems in water to reveal <120 fs and 1.5 ps electron injection times along with 30% slower back electron transfer time for the ruthenium complex **3**. However, the corresponding osmium complex **4** shows strikingly different behavior for which only a <120 fs ultrafast injection is observed. Most remarkably, the back electron transfer is faster as compared to the corresponding catechol analogue of the dye. The origin and the consequences of such profound effects on the ultrafast interfacial dynamics are discussed. This Article on the electron transfer dynamics of the aforesaid systems reinforces the possibility of resorcinol being explored and developed as an extremely efficient binding moiety for use in dye-sensitized solar cells.

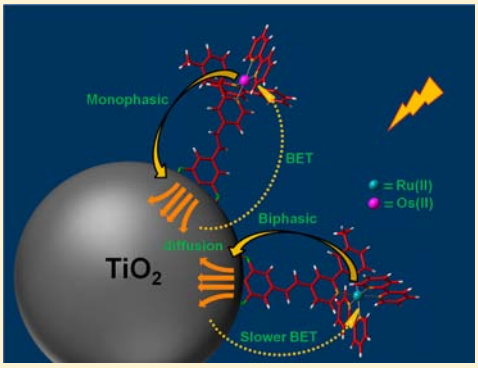


## 1. INTRODUCTION

Contemporary literature reinforces the importance of optimization of the interfacial electron transfer parameters in the design of a resourceful dye-sensitized solar cell.[1] This elementary yet complex process has therefore attracted a large number of research groups who are involved in an effort to understand and control the sensitization events.[2]

Sensitization of a semiconductor is achieved by chemical anchoring of dye molecules to the semiconductor nanosurface. The choice of anchoring groups, for example, carboxyl, phosphonate (the ones most explored), acetylacetonate, has been shown to significantly influence the interfacial electron transfer dynamics, and extensive studies have consequently been done in this regard.[3]

However, in water the stability of the carboxyl and the phosphonate ester linkages is limited to a small range of pH values due to the related protolytic equilibrium.[4] In aqueous solutions of higher pH, hydrolysis and subsequent dechelation of the anchoring group from the Ti(IV) groups in $TiO_2$ can occur on the surface. Most often, equilibration of the surface titanol groups takes place quite slowly so that dechelation shows only in a few long-term stability tests. The pH range where the devices can be used in aqueous media is rather limited for this reason.[5] This led to the development of acetylacetonates and catecholates as anchoring groups, most importantly, catecholates, which have considerably higher $pK_a$ values, and hence chances of dechelation are greatly reduced.[3j,6]

Despite the above fact, sensitizer dyes with catecholate anchoring groups have failed to compete successfully with those with carboxylate and phosphonate anchors, in terms of their energy conversion efficiencies.[6a] This is because the interfacial electron transfer reaction in such ene-diol bound $TiO_2$ systems falls in the nonergodic regime because of a very strong coupling of the dye with the semiconductor. In a nonergodic system, the reaction proceeds before electronic, vibrational, and rotational energy equilibration over all of the degrees of freedom.[7] If the electron injection process at the dye−semiconductor interface is really faster than the intramolecular energy relaxation processes such as vibrational relaxation, internal conversion, and intersystem crossing, then the surplus vibronic energy of the photo-excited sensitizer molecule is dispelled quickly into the semiconductor particle, thus preventing parallel destructive side reactions that might influence the long-term stability of the system. Thus, a nonergodic electron injection pathway in a dye-sensitized $TiO_2$ nanoparticle system implies the prospect of complete utilization of the energy of the photon.[8] Indeed, solar energy conversion in dye-sensitized devices is most efficient when operating in the nonergodic limit.[2j] However, this nonergodicity in the electron transfer for catecholate bound $TiO_2$ systems can seldom be harvested. This is because of the very strong coupling of the dye with the semiconductor, which

**Received:** February 5, 2013
**Published:** April 5, 2013

   dx.doi.org/10.1021/ic4003548 | *Inorg. Chem.* 2013, 52, 5366−5377

**Scheme 1. Molecular Structures of 3 and 4**

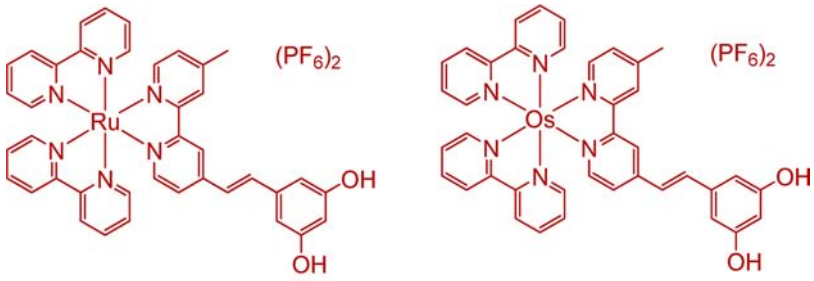


manifests itself not only in an ultrafast forward electron transfer but also in the very fast backward electron transfer (BET) rates, rates that are much faster than dyes with carboxylic anchors.[3f−h,6b,9]

Several approaches have been adopted by our research group in this regard to slow this BET rate appreciably. Secondary electron-donating groups have been appended to the primary Ru(II) redox center[9e] following numerous earlier works by Meyer and colleagues and also Grätzel and colleagues involving carboxylate and phosphonate bound dyes.[10] The effects of these groups are however superseded by the extremely fast charge recombination rates of catecholate binding. A related study suggested that Ru(II)−polypyridyl complexes comprising of ligand-localized charge transfer (LLCT) states can be a better photosensitizer in terms of improved electron injection yield and slow BET processes than complexes comprised of metal to ligand charge transfer (MLCT) states.[11] However, the complicated synthetic procedure of these complexes always places a question mark on practical applicability. Another of our studies employed sequential energy and electron transfer in a catecholate bound Ru−Os−Ru hybrid sensitizer molecule, and a slower BET rate could be obtained.[12] This slow BET rate was argued to be associated with the delocalization of the hole in the trinuclear complex radical cation. However, such big molecules again present serious impediments during syntheses and also lead to an obvious lower surface coverage and might consequently lead to lower photocurrent yields. The development of an ene-diol tagged viable sensitizer system therefore still remains a busy plinth of modern research in this area.

This problem of fast BET because of the very strong binding in such catecholate bound systems is presumably because of the hydroxyl groups binding to $TiO_2$ in a very localized manner, that is, to a single $Ti^{4+}$ atom forming a five-membered chelate ring.[13] If the binding of the enediol dye is made to involve multiple $Ti^{4+}$ centers, then the overlap of the dye LUMO with the Ti 3d orbital network would not be that localized, and one can expect the effective binding to become weaker. Binding of the dye to multiple $Ti^{4+}$ centers is also expected to enhance the electron delocalization in the $TiO_2$ nanocrystal after initial electron injection, which in turn is expected to decrease the BET rate.

To explore this hypothesis, an innovative ruthenium(II)-, osmium(II)-, rhenium(I)-polypyridyl-based sensitizer system containing resorcinol instead of catechol as the enediol anchor has been developed. Our very recent work on the ultrafast interfacial electron transfer dynamics of the ruthenium(II)- and rhenium(I)-polypyridyl complexes on oleic acid capped $TiO_2$ in chloroform has indeed corroborated our hypothesis.[14] As a part of our continuing research on the ultrafast dynamics of such resorcinol bound dye−$TiO_2$ systems, we report herein the effect of the alteration in the anchoring moiety as discussed above on the interfacial electron transfer dynamics of the ruthenium(II)/osmium(II)-polypyridyl complexes, **3** and **4**, respectively (Scheme 1), in aqueous environment, as probed by femtosecond transient absorption spectroscopic study. This study is therefore the first report on the synthesis of ruthenium(II)/osmium(II)-polypyridyl-resorcinol dyes and is the only report on the time-resolved femtosecond transient absorption spectroscopy of osmium(II)-polypyridyl-resorcinol dye on the $TiO_2$ surface. In addition, we believe that the present work would add significantly to the ongoing research efforts toward the development of aqueous dye-sensitized photoelectrochemical fuel cells.[1g−i]

## 2. EXPERIMENTAL SECTION

**a. Materials.** Titanium(IV) tetraisopropoxide (97%), isopropyl alcohol, 4,4′-dimethyl-2,2′-bipyridine, *n*-butyl lithium, 3,5-dimethoxybenzaldehyde, 2,2′-bipyridine, ruthenium trichloride hydrate, ammonium hexachloro osmate and Dowex MR-3 mixed bed ion-exchange resin have been obtained from Sigma-Aldrich and used as received. Solvents like THF, pyridine and isopropyl alcohol have been dried and distilled prior to use. Nanopure water (Barnsted System, U.S.) has been used for making all aqueous solutions. All other reagents (AR grade) have been procured from S. D. Fine Chemicals (India). Solvents have been degassed thoroughly with IOLAR grade dinitrogen gas before use in the preparation of standard solutions. $Ru(bpy)_2Cl_2$,[15] $Os(bpy)_2Cl_2$,[16] **5**[6b] and **6**[17] have been prepared following previously reported procedures.

**b. Analytical Methods.** FTIR spectra have been recorded as KBr pellets in a cell fitted with a KBr window, using a Perkin-Elmer Spectra GX 2000 spectrometer. $^1H$ NMR spectra have been recorded on a Bruker 200 MHz FT NMR (model: Avance-DPX 200) using tetramethylsilane (TMS) as an internal standard. ESI−MS measurements have been carried out on a Waters QTof-Micro instrument. Microanalyses (C, H, N) have been performed using a Perkin-Elmer 4100 elemental analyzer. Electronic spectra have been recorded with a Varian Cary 500 UV−vis−NIR spectrophotometer; room-temperature luminescence spectra have been recorded with an Edinburgh Xe 900 luminescence spectrofluorimeter, fitted with a red-sensitive photomultiplier tube. Electrochemical experiments have been performed in acetonitrile using a bipotentiostat (AFCPBI, PINE Instrument Co.) electrochemical instrument with a conventional three-electrode cell assembly. An Ag/AgCl, saturated KCl reference and a platinum working electrode have been used for all measurements. Ferrocene has been used as an internal standard. It is more conventional to report the potential values vs NHE while reporting and comparing interfacial electron transfer dynamics. All potentials have therefore been quoted with respect to the normal hydrgen electrode in water.[18]

**c. Femtosecond Visible Spectrometer.** The femtosecond tunable visible spectrometer has been developed based on a multipass amplified femtosecond Ti:sapphire laser system supplied by Thales, France.[19] The pulses of 20 fs duration and 4 nJ energy per pulse at 800 nm, obtained from a self-mode-locked Ti:sapphire laser oscillator


dx.doi.org/10.1021/ic4003548 | Inorg. Chem. 2013, 52, 5366−5377

(Synergy 20, Femtolaser, Austria), are amplified in a regenerative and two-pass amplifier pumped by a 20 W DPSS laser (JADE) to generate 40 fs laser pulses of about 1.2 mJ energy at a repetition rate of 1 kHz. The 800 nm output pulse from the multipass amplifier is split into two parts to generate pump and probe pulses. In the present investigation, we have used frequency doubled 400 nm as the excitation sources. To generate pump pulses at 400 nm, one part of the 800 nm output with 200 $\mu$J/pulse is frequency doubled in BBO crystals. To generate visible probe pulses, about 3 $\mu$J of the 800 nm beam is focused onto a 1.5 mm thick sapphire window. The intensity of the 800 nm beam is adjusted by iris size and ND filters to obtain a stable white light continuum in the 400−1000 nm region. The probe pulses are split into the signal and reference beams and are detected by two matched photodiodes with variable gain. We have kept the spot sizes of the pump beam and probe beam at the crossing point around 500 and 300 $\mu$m, respectively. The noise level of the white light is about ∼0.5% with occasional spikes due to oscillator fluctuation. We have noticed that most laser noise is low-frequency noise and can be eliminated by comparing the adjacent probe laser pulses (pump blocked vs unblocked using a mechanical chopper). The typical noise in the measured absorbance change is about <0.3%. The instrument response function (IRF) for 400 nm excitation has been obtained by fitting the rise time of the bleach of sodium salt of meso-tetrakis(4-sulfonatophenyl)porphyrin (TPPS) at 710 nm and has been found to be 120 fs. The data analysis and fitting at individual wavelengths have been done with the LabView program.

**d. Synthesis of $TiO_2$ Nanoparticles.** $TiO_2$ nanoparticles have been prepared by controlled hydrolysis of titanium(IV) tetraisopropoxide.[20] A solution of 5 mL of $Ti[OCH(CH_3)_2]_4$ (Aldrich, 97%) in 95 mL of isopropyl alcohol is added dropwise (1 mL/min) to 900 mL of nanopure water (2 °C) at pH 1.5 (adjusted with $HNO_3$). The solution is continuously stirred for 10−12 h until the formation of a transparent colloid. The colloidal solution is concentrated at 35−40 °C with a rotary evaporator and then dried with nitrogen stream to yield a white powder. The transmission electron microscopy (TEM) images show the particle size to be ∼3 nm, and specific area electron diffraction (SAED) pattern confirms the particles to be crystalline anatase (Figure S1). In the present work, all colloidal samples (15 g/L) have been prepared following an already reported procedure.[21]

**e. Preparation of Sample Solution.** The complexes discussed are insoluble in water, and so sensitization has been done by dissolving them in the least possible volume of acetonitrile (this volume is less than 1% of the total volume) and then by adding the dissolved dye into an aqueous colloidal solution of the nanoparticles. The resulting solutions are stirred for one-half an hour and then kept in dark overnight for the dye to covalently bind to $TiO_2$. For all of the measurements, the sample solutions have been deoxygenated by continuously bubbling high-purity nitrogen (99.95 IOLAR grade from Indian Oxygen Co. Ltd., India) through the solutions.

**f. Synthesis.** *i. 4-(3,5-Dimethoxystyryl)-4′-methyl-2,2′-bipyridine (1).* To a solution of 4,4′-dimethyl-2,2′-bipyridine (1.84 g, 10 mmol) in ice-cold THF (30 mL) under $N_2$ is added a solution of lithium diisopropylamide (10 mmol; freshly prepared by mixing 6.65 mL of 1.6 M *n*-BuLi in hexanes and 1.325 mL of dry diisopropylamine at room temperature under $N_2$) dropwise over 15 min. The deep chocolate brown solution is stirred at 0 °C for 1 h, after which a solution of 3,5-dimethoxybenzaldehyde (1.66 g, 10 mmol) in THF (20 mL) is added dropwise while maintaining the temperature at −30 °C. The mixture is allowed to warm to room temperature and stirred overnight. After quenching the reaction with water and evaporation to dryness in vacuum, an oily mass is obtained. This is dissolved in chloroform and solvent extraction is done to remove the ionic impurities. The organic layer is dried with anhydrous sodium sulfate and evaporated to give a crude oily residue (the crude intermediate alcohol) which is used without purification for the subsequent dehydration. The oil is dissolved in dry pyridine (50 mL) and a solution of $POCl_3$ (1.16 mL, 12.5 mmol) in dry pyridine (50 mL) is added dropwise under $N_2$ at room temperature with vigorous stirring. After 1 h, the pyridine is evaporated in a vacuum and crushed ice is added; the mixture is left for 30 min to ensure that all residual $POCl_3$ is destroyed. The pH of the aqueous solution is adjusted to between 3 and 4 and unwanted organic materials are extracted with $CH_2Cl_2$. The aqueous solution is then made just alkaline (pH ≈ 8) and the crude products are extracted into $CH_2Cl_2$, which is subsequently dried with anhydrous sodium sulfate and evaporated to give a yellowish brown solid. This is purified by column chromatography over silica using chloroform/methanol as the eluent to give the desired product in pure form. Yield: 1.66 g, 50%. ESI−MS ($m/z$): calculated for $C_{21}H_{20}N_2O_2$, 332.15; observed, 333.27 $[M + 1]^+$. $^1$H NMR (200 MHz, $CDCl_3$): $\delta$ (ppm) 8.39 (1H, d, $J$ = 5 Hz, $H^{6'}$ (bpy)); 8.35 (1H, d, $J$ = 5 Hz, $H^{5'}$ (bpy)); 8.30 (1H, s, $H^{3'}$ (bpy)); 8.06 (1H, s, $H^3$ (bpy)); 7.09 (1H, d, $J$ = 13.2 Hz, $H^{ethenyl}$); 7.05−7.02 (1H, m, $H^6$ (bpy)); 6.87 (1H, d, $J$ = 5 Hz, $H^5$ (bpy)); 6.80 (1H, d, $J$ = 16.4 Hz, $H^{ethenyl}$); 6.47 (2H, d, $J$ = 2 Hz, $H^2$(phenyl)); 6.24−6.21 (1H, m, $H^4$(phenyl)); 3.57 (6H, s, $-OCH_3$); 2.17 (3H, s, $-CH_3$). IR (KBr pellet, $cm^{-1}$): 1591 ($\nu$(C=C)), 1056 ($\nu$(C−O)). Anal. Calcd for $C_{21}H_{20}N_2O_2$: C, 75.88; H, 6.06; N, 8.43. Found: C, 75.5; H, 6.26; N, 8.47.

*ii. 5-(2-(4′-Methyl-2,2′-bipyridin-4-yl)vinyl)benzene-1,3-diol (2).* 32 mL of analytical grade pyridine is taken in a round bottomed flask equipped for distillation, and 35.2 mL of concentrated hydrochloric acid is added to it with continuous stirring. This mixture is then heated for 2 h at 220 °C to distill off the water from the mixture. After the mixture was cooled to 140 °C, **1** (1 g, 3.01 mmol) is added as a solid, and the reaction mixture is stirred and heated at 200 °C for 4 h. The reaction mixture is then cooled, and 30 mL of water is added to dissolve the crude mixture. The pH of the resulting solution is then raised to 6−6.5 by slowly adding a dilute solution of caustic soda to precipitate the desired compound. This precipitate is then filtered through a grade 4 sintered glass crucible, washed with large volumes of water, and dried overnight in a vacuum desiccator to give compound **2** in pure form. Yield: 870 mg, 95%. ESI−MS ($m/z$): calculated for $C_{19}H_{16}N_2O_2$, 304.12; observed, 305.4 $[M + 1]^+$. $^1$H NMR (200 MHz, $CD_3CN$): $\delta$ (ppm) 8.58 (1H, d, $J$ = 5.2 Hz, $H^{6'}$ (bpy)); 8.53 (1H, d, $J$ = 5 Hz, $H^{5'}$ (bpy)); 8.38 (1H, s, $H^{3'}$ (bpy)); 8.16 (1H, s, $H^3$ (bpy)); 7.57 (1H, d, $J$ = 5 Hz, $H^6$ (bpy)); 7.42 (1H, d, $J$ = 16.2 Hz, $H^{ethenyl}$); 7.33 (1H, d, $J$ = 4.6 Hz, $H^5$ (bpy)); 7.13 (1H, d, $J$ = 16.4 Hz, $H^{ethenyl}$); 6.59−6.58 (2H, m, $H^2$(phenyl)); 6.28−6.26 (1H, m, $H^4$(phenyl)); 2.49 (3H, s, $-CH_3$). IR (KBr pellet, $cm^{-1}$): 3430 ($\nu$(OH)), 1589 ($\nu$(C=C)). Anal. Calcd for $C_{19}H_{16}N_2O_2$: C, 74.98; H, 5.3; N, 9.2. Found: C, 75.2; H, 5.15; N, 9.1.

*iii. {Bis-(2,2′-bpy)-(5-[2-(4′-methyl-2,2′-bipyridin-4-yl)vinyl]-benzene-1,3-diol)} Ruthenium(II) Hexafluorophosphate (3).* $Ru(bpy)_2Cl_2{\cdot}2H_2O$ (86 mg, 0.165 mmol) and **2** (50.2 mg, 0.165 mmol) are refluxed in ethanol for 8 h with continuous stirring. The solvent is then evaporated and the product is made soluble in a minimum volume of water. Saturated aqueous $NH_4PF_6$ (10 mol equivalents) is added to the resulting solution to precipitate the desired Ru(II)-polypyridyl complex as the hexafluorophosphate salt. This is kept as such for 4−5 h in a refrigerator to ensure complete precipitation after which it is filtered, washed with large volumes of cold water and dried in a vacuum desiccator. The crude compound so obtained is purified by column chromatography over silica using acetonitrile/water/saturated aqueous $KPF_6$ as the eluent. The second fraction is collected and the solvent is removed to isolate a red solid, which is redissolved in dichloromethane and two drops of acetonitrile, and solvent extraction is done to remove the excess $KPF_6$ used in the eluent. The organic phase is dried over anhydrous sodium sulfate and is evaporated to dryness to give the desired product in pure form. Yield: 58.3 mg (35%). ESI-MS ($m/z$): calculated for $C_{39}H_{32}N_6O_2PF_6Ru$, 863.09 $[M - PF_6^-]^{+'}$ observed, 863.41 $[M - PF_6^-]^+$. $^1$H NMR (200 MHz, $CD_3CN$): $\delta$ (ppm) 8.62−8.58 (1H, m, $H^{6'}$ (bpy-res)); 8.53−8.50 (2H, m, $H^6$ (bpy) and/or $H^{6'}$ (bpy); 8.49−8.46 (2H, m, $H^6$ (bpy) and/or $H^{6'}$ (bpy)); 8.09−8.01 (4H, m, $H^3$ (bpy) and $H^{3'}$ (bpy)); 7.81 (1H, d, $J$ = 5.6 Hz, $H^4$ (bpy) or $H^{4'}$ (bpy)); 7.75−7.68 (3H, m, $H^4$ (bpy) and $H^{4'}$ (bpy)); 7.60 (1H, d, $J$ = 4.6 Hz, $H^{5'}$ (bpy-res)); 7.55−7.49 (2H, m, $H^{3'}$ (bpy-res) and $H^{ethenyl}$); 7.43−7.36 (5H, m, $H^5$ (bpy) and $H^{5'}$ (bpy), $H^3$ (bpy-res)); 7.29−7.22 (3H, m, $H^5$ (bpy-res) and $H^6$ (bpy-res), $H^{ethenyl}$); 6.62 (2H, d, $J$ = 2 Hz, $H^2$(phenyl)); 6.34 (1H, t, $J$ = 2 Hz, $H^4$(phenyl)); 2.56 (3H, s, $-CH_3$(bpy-res)). IR (KBr pellet, $cm^{-1}$): 3432 ($\nu$(OH)), 1606 ($\nu$(C=


dx.doi.org/10.1021/ic4003548 | Inorg. Chem. 2013, 52, 5366−5377

**Scheme 2. Reaction Scheme for the Synthesis of 3 and 4**[a]

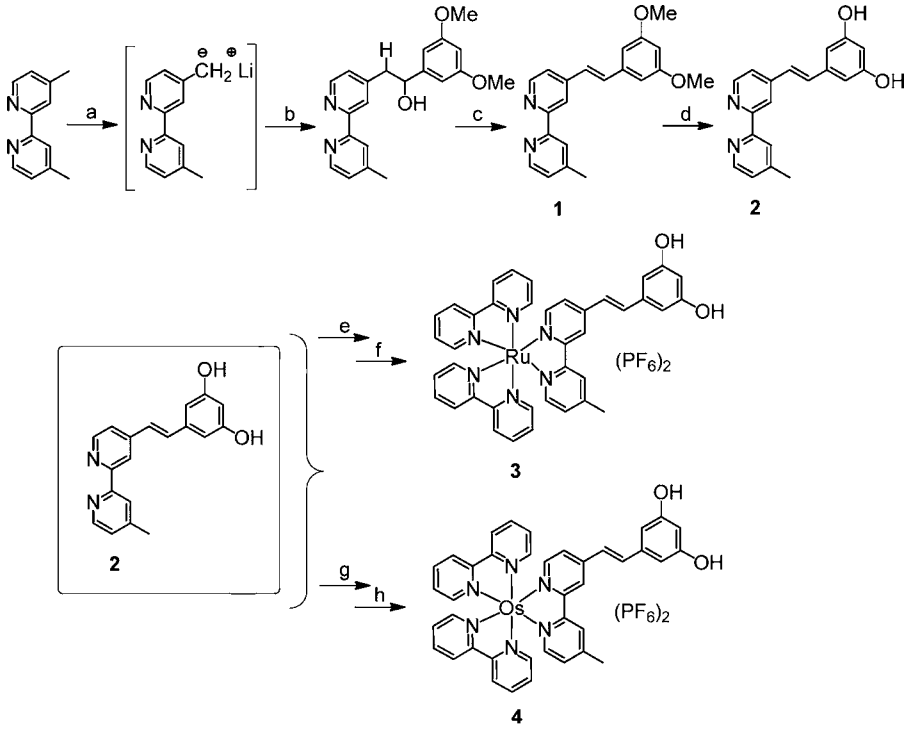


[a]a = LDA, THF, 0 °C; b = 3,5-dimethoxybenzaldehyde, THF, −30 °C; c = $POCl_3$, pyridine, room temperature; d = pyridine, HCl, 200 °C; e = $Ru(bpy)_2Cl_2{\cdot}2H_2O$, EtOH, reflux; f = saturated aqueous $NH_4PF_6$; g = $OS(bpy)_2Cl_2$, EtOH, reflux; h = saturated aqueous $NH_4PF_6$.

C)), 840 ($\nu(PF_6)$). Anal. Calcd for $C_{39}H_{32}N_6O_2P_2F_{12}Ru$: C, 46.48; H, 3.20; N, 8.34; Found: C, 46.47; H, 3.18; N, 8.38.

*iv. {Bis-(2,2′-bpy)-(5-[2-(4′-methyl-2,2′-bipyridin-4-yl)vinyl]-benzene-1,3-diol)} Osmium(II) Hexafluorophosphate (4).* This is prepared by a similar procedure as adopted for the synthesis of **3**. $Os(bpy)_2Cl_2{\cdot}2H_2O$ (100 mg, 0.165 mmol) and **2** (50.2 mg, 0.165 mmol) are refluxed in ethanol for 8 h with continuous stirring. The solvent then is evaporated and the product is made soluble in a minimum volume of water. Saturated aqueous $KPF_6$ (10 mol equiv) is added to the resulting solution to precipitate the desired Os(II)-polypyridyl complex as the hexafluorophosphate salt. This is kept as such for 4−5 h in a refrigerator to ensure complete precipitation, after which it is filtered, washed with cold water and dried in a vacuum desiccator. The crude compound so obtained is purified by column chromatography over alumina using acetonitrile/water/saturated aqueous $KPF_6$ as the eluent. The last fraction is collected and the solvent is removed to isolate a greenish-black solid, which is redissolved in dichloromethane and two drops of acetonitrile and solvent extraction is done to remove the excess $KPF_6$ used in the eluent. The organic phase is dried over anhydrous sodium sulfate and is evaporated to dryness to give the desired product. Yield: 57.6 mg (32%). ESI−MS ($m/z$): calculated for $C_{39}H_{32}N_6O_2PF_6Os$, 953.15 $[M - PF_6^-]^+$; observed, 953.34 $[M - PF_6^-]^+$, 404.18 $[M - 2PF_6^-]^{2+}$. $^1H$ NMR (200 MHz, $CD_3CN$): $\delta$ (ppm) 8.57−8.49 (1H, m, $H^{6'}$ (bpy-res)); 8.51−8.47 (2H, m, $H^6$ (bpy) and/or $H^{6'}$ (bpy); 8.47−8.43 (2H, m, $H^6$ (bpy) and/or $H^{6'}$ (bpy)); 7.89−7.81 (4H, m, $H^3$ (bpy) and $H^{3'}$ (bpy)); 7.71 (1H, d, $J$ = 5.6 Hz, $H^4$ (bpy) or $H^{4'}$ (bpy)); 7.66−7.62 (3H, m, $H^4$ (bpy) and $H^{4'}$ (bpy)); 7.54 (1H, d, $J$ = 4.6 Hz, $H^{5'}$ (bpy-res)); 7.50−7.42 (2H, m, $H^{3'}$ (bpy-res) and $H_{ethenyl}$); 7.34−7.25 (5H, m, $H^5$ (bpy) and $H^{5'}$ (bpy), $H^3$ (bpy-res)); 7.21−7.13 (3H, m, $H^5$ (bpy-res) and $H^6$ (bpy-res), $H^{ethenyl}$); 6.61 (2H, d, $J$ = 2 Hz, $H^2$(phenyl)); 6.32 (1H, t, $J$ = 2 Hz, $H^4$(phenyl)); 2.64 (3H, s, $-CH_3$(bpy-res)). IR (KBr pellet, $cm^{-1}$): 3433 ($\nu$(OH)), 1608 ($\nu$(C=C)), 838 ($\nu(PF_6)$). Anal. Calcd for $C_{39}H_{32}N_6O_2P_2F_{12}Os$: C, 42.7; H, 2.94; N, 7.66. Found: C, 42.6; H, 2.9; N, 7.8.

## 3. RESULTS AND DISCUSSION

The synthetic methodology adopted for the synthesis of **3** and **4** is shown in Scheme 2. The synthesis of **1** is done via a lithium diisopropyl amide-mediated C−C bond formation reaction to give the precursor alcohol, which is dehydrated to **1** using $POCl_3$ in pyridine solvent that itself acts as the base. Removal of the methyl group in **1** is done with molten pyridinium hydrochloride to give **2**.

The final ruthenium- and osmium-complexes, **3** and **4**, are prepared by reactions of **2**, respectively, with $Ru(bpy)_2Cl_2$ and $Os(bpy)_2Cl_2$ in ethanol. The purity of the complexes is checked by different analytical and spectroscopic methods and the analytical data match well with that of the expected formulation. 2,2′-Bipyridine (bpy) ligands are employed to make sure that the MLCT excited state has electrons localized on the surface-bound ligand for all of the sensitizers. This is because the surface-bound ligand, that is, the bipyridine ligand with appended resorcinol moiety, because of its extended conjugated structure, is energetically low lying as compared to the unsubstituted bipyridine ligands (vide infra). As a result of the low lying nature of the surface-bound bipyridine-resorcinol ligand in **3** and **4**, upon excitation, population of the corresponding MLCT state is expected to dominate over that constituted by the other unsubstituted ligands. Moreover, the unsubstituted 2,2′-bpy ligands being at higher energies, electron density from these ligands is expected to get transferred to the surface-bound bipyridine-resorcinol ligand with time.

Absorption and emission spectra recorded for **3** and **4** in water:acetonitrile 99:1 (v/v) medium are shown in Figure 1. The absorption spectrum is characterized by strong ligand centered $\pi-\pi^*$ transitions at 288 and 296 nm for **3** and **4**, respectively; while the band at 330 nm can be assigned either to delocalized interligand charge transfer or to metal centered


dx.doi.org/10.1021/ic4003548 | Inorg. Chem. 2013, 52, 5366−5377

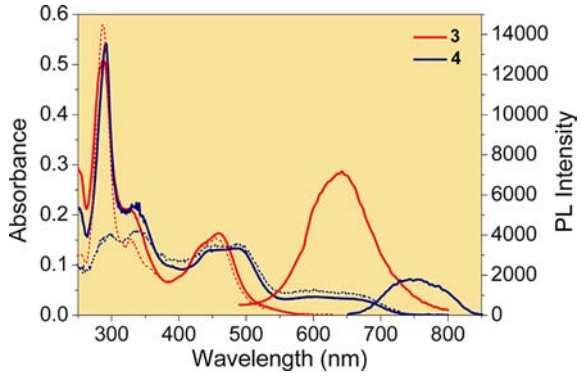


**Figure 1.** Absorption and emission spectra of **3** (red) and **4** (blue) in water:acetonitrile 99:1 (v/v) medium. The concentrations of both **3** and **4** are $1 \times 10^{-5}$ M. The dotted lines show the normalized excitation spectra.

(MC) transitions.[22] The familiar metal to ligand charge transfer comprised of overlapping $^1$MLCT based $d_{M(II)} \rightarrow \pi^*_{bpy}$ [M = Ru(II)/Os(II)] manifests in the low energy broad absorption band peaking at 460 nm for **3** ($\varepsilon = 1.58 \times 10^4$ M$^{-1}$ cm$^{-1}$) and at 488 nm for **4** ($\varepsilon = 1.44 \times 10^4$ M$^{-1}$ cm$^{-1}$).[22] The Os(II) center, as compared to the Ru(II) center, is characterized by a significantly higher spin orbit coupling, and this is responsible for the allowedness of the spin forbidden $^3$MLCT based $d_{Os(II)} \rightarrow \pi^*_{bpy}$ transition,[2h,22b] resulting in another broad absorption between 550 and 710 nm for **4** ($\varepsilon_{500} = 1.437 \times 10^4$ M$^{-1}$ cm$^{-1}$, $\varepsilon_{630} = 3730$ M$^{-1}$ cm$^{-1}$). The emission spectrum of **3** consists of a broad $^3$MLCT-based emission with $\lambda_{max}$ at 640 nm when excited at 460 nm. For **4**, this emission peaks at $\lambda_{max} = 750$ nm when excited at either 488 or 630 nm.

Excitation spectra of **3** and **4** (Figure 1) agree well with their respective absorption and absorptance spectra (Figure S2), indicating that the observed photoluminescence is from the sensitizers.[3h]

Electrochemical studies on **3** (Figure 2) reveal a reversible $Ru^{2+}/Ru^{3+}$ redox couple at 1.25 V ($\Delta E = 69$ mV) (vide supra),

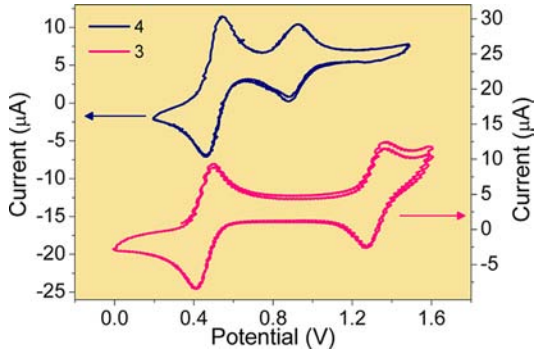


**Figure 2.** Cyclic voltammogram of **3** (pink, right-hand side layer in figure) and **4** (navy blue, left-hand side layer in figure) in acetonitrile. Ag/AgCl (saturated KCl) has been used as the reference electrode. Scan rate for both of the scans is 100 mV/s. Ligand-based reductions are omitted because only the metal-based redox potentials have been used in the interpretation of data throughout this Article. The peak on the left side in both of the voltammograms is due to the ferrocene/ferrocenium couple, which has been added as an internal standard. A difference in the concentrations of potassium chloride solutions in the reference electrodes presumably causes the difference in the $E_{1/2}^{Fc/Fc+}$ values in the two voltammograms.

and only two bipyridyl centered reductions can be observed at −1.39 and −1.52 V in the +2 to −2 V potential window available. For **4**, the $Os^{2+}/Os^{3+}$ reversible redox couple appears at 0.8 V ($\Delta E = 58$ mV) (Figure 2) and bipyridyl centered reductions can be seen at −1.37 and −1.58 V. An important point to note is that the metal centered redox potential values in these resorcinol dyes are significantly more negative than the respective catechol dyes, **5** and **6** (Scheme 3).

For **5**, the $Ru^{2+}/Ru^{3+}$ redox couple appears at 1.32 V, while the $Os^{2+}/Os^{3+}$ redox couple appears at 1.14 V in **6**.[6b,17] Intra- and/or intermolecular hydrogen bonding is expected to be more prominent for the catechol moiety in **5** and **6** than in the resorcinol counterpart in **3** and **4**. Probably a greater participation of the catechol moiety in this aforesaid hydrogen bonding curtails the electron density from active involvement in +R resonance effects toward the sensitizer core in **5** and **6**.[23] This effect, being most likely less dominant for the resorcinol moiety in **3** and **4**, is presumably being reflected in lower values of the metal centered redox potentials. Also, this effect is most likely more prominent in case of the Os(II)-based dyes, and hence a greater difference in the potential values is seen.

Knowledge about the position of the excited state of the dye with respect to the conduction band of $TiO_2$ is essential to comprehend the feasibility of electron injection from the dye to the semiconductor nanoparticles.

$E_{0-0}$ transition energies for the $^3$MLCT states of **3** and **4** are calculated to be 2.16 and 1.78 eV, respectively, from the respective excitation and emission spectra. The excited-state potentials $E(S^+/S^*)$ are thus −0.91 and −0.98 V for **3** and **4**, respectively, following the equation $[E(S^+/S^*)] = [E(S^+/S)] - E_{0-0}$.[9e,24] The $E_{0-0}$ values for the $^1$MLCT states are approximated to be 2.41 and 2.21 eV for **3** and **4**, respectively, from the onset of optical absorption (unlike the estimation of $E_{0-0}$ for $^3$MLCT states, which have been done as stated above). The corresponding excited-state potentials are thus −1.16 and −1.41 V for **3** and **4**, respectively. The excited-state potentials being above the conduction band level, electron injection from the excited state of the sensitizers into the conduction band of $TiO_2$ becomes thermodynamically feasible.[25]

The absorption spectrum becomes broad with simultaneous increase in absorbance on steady addition of an aqueous solution of $TiO_2$ nanoparticles to the aforesaid complexes (Figure 3a and b), which indicates significant interaction of the dye molecules with the $TiO_2$ nanoparticles. Unlike many dyes with pendant catechol groups for binding to $TiO_2$, no new charge transfer band appears.[9a,d,26] This suggests weaker electronic coupling of the resorcinol dyes, **3** and **4**, to $TiO_2$ than the catechol dyes **5** and **6**. However, the fact that the MLCT absorption does become broad and the OD increases only means that charge transfer interaction is there, but the binding is probably not strong enough to manifest this CT interaction as a new band.[6b,9b,c,e,10e,11,12,17] This conclusion is further supported by the fact that the emission spectra of **3** and **4** in solution are identical to that on $TiO_2$.

However, the emission intensity is radically diminished on $TiO_2$ surface (Figure 4) ($TiO_2$ concentration is only 5 g/L for the fluorescence spectra in Figure 4 as compared to 15g/L for the transient absorption studies), suggesting substantial quenching of the excited state by electron injection[3f,9c,e,10e,17] and hence negligible contribution of excited-state features in the transient absorption data on $TiO_2$ (vide infra).

For a comprehensive understanding of the electron transfer dynamics of **3** and **4** on $TiO_2$ nanoparticle surface, a detailed


dx.doi.org/10.1021/ic4003548 | Inorg. Chem. 2013, 52, 5366−5377

**Scheme 3. Molecular Structures of 5 and 6**

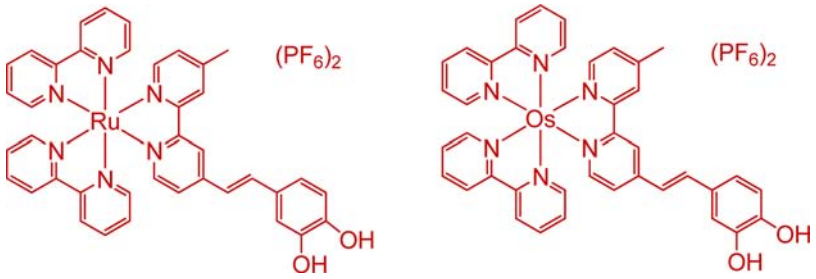


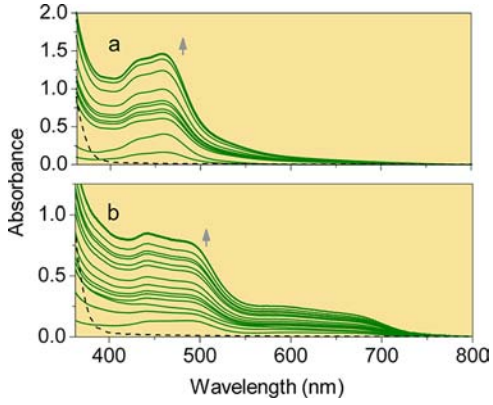


**Figure 3.** Changes in absorbance of (a) **3** ($1.034 \times 10^{-5}$ M) on $TiO_2$ (0–4.06 g/L) and (b) **4** ($0.9266 \times 10^{-5}$ M) on $TiO_2$ (0–3.52 g/L) in water:acetonitrile 99:1 (v/v) medium. Shown as a dashed line is the spectral profile of $TiO_2$ (15 g/L) in water:acetonitrile 99:1 (v/v) medium.

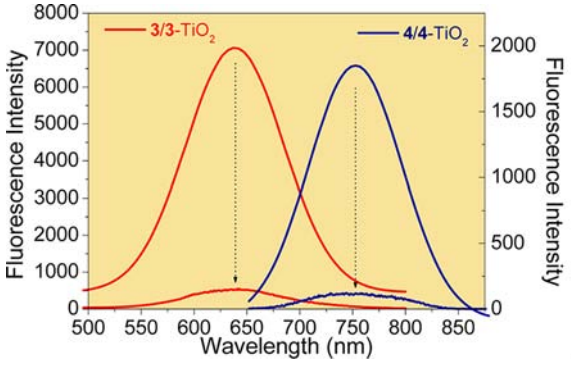


**Figure 4.** Fluorescence quenching of **3** ($1 \times 10^{-5}$ M) (left layer, red) and **4** ($1 \times 10^{-5}$ M) (right layer, blue) on $TiO_2$ (5 g/L) water:acetonitrile 99:1 (v/v) medium.

study of the excited-state dynamics of the free sensitizer molecules is essential. Transient absorption spectrum has been recorded both in acetonitrile and in water:acetonitrile 99:1 (v/v), and the kinetic data are very similar in the two solvents. Figure 5 shows the transient absorption spectrum of **3** in water:acetonitrile 99:1 (v/v) medium. The transient absorption spectrum of **3** shows a broad absorption ranging from 500 to 1000 nm. Recent work by Chergui et al. employing broadband fluorescence spectroscopy has revealed that intersystem crossing in ruthenium polypyridyl complexes occurs in 15 ± 10 fs.[27] The absorption feature, therefore, in the transient absorption spectrum can be assigned to excited triplet state absorption.[6b,9a–c,11] This is accompanied by a simultaneous

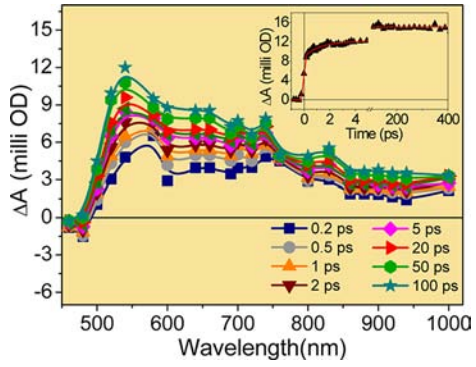


**Figure 5.** Transient absorption spectrum of **3** at different delay times in water:acetonitrile 99:1 (v/v) medium measured after 400 nm (fwhm <120 fs) excitation. Concentration of **3** is ~200 $\mu$M. Shown in the inset is the kinetic trace for **3** monitored at 900 nm.

negative absorption due to the ground-state bleach below 500 nm.[6b,9a,b,11]

The kinetic trace of **3** at 900 nm (Figure 5 inset) shows a 1 ps (19.2%) and a 25 ps (23.2%) increase in oscillator strength after the initial excited-state population occurring in pulse width limited time (<120 fs, +57.6%). McCusker et al. studied the ultrafast dynamics of the excited-state evolution of a series of ruthenium polypyridyl complexes pumping at 400 nm and could observe a 5 ps component in the pump–probe difference absorption kinetics monitored at 532 nm that they assigned as the vibrational cooling dynamics in the $^3$MLCT excited state.[28] Their assignment was corroborated by the fact that similar dynamics could again be observed for a comparable complex when excited with a 400 nm pump and probed at 510 nm; while with 480 nm pump at the same probe wavelength the complex did not show any dynamics beyond 200 fs.[29] Interestingly, in the complex with appended phenyl rings, the component due to vibrational cooling decreased to 2 ps because of the phenyl ring rotation that acted as an easy pathway for dispelling the excess vibrational energy. Therefore, considering the non rigid structure and also the appended hydroxyl groups that might arbitrate additional relaxation pathways, more so in solvent water, it would not be injudicious to assign the 1 ps component to vibrational relaxation in the $^3$MLCT manifolds. In addition, the average solvation relaxation time, $\langle\tau_s\rangle$, in water and in acetonitrile is reported to be ~500–600 fs.[30] This and the fact that on $TiO_2$ surface we have a similar 1.5 ps injection component whose amplitude is probe wavelength dependent (vide infra) rule out the possibility of this component in the free dye arising due to solvation. This assignment is further corroborated by the appearance of a similar 0.7 ps in the dynamics of **3** in methanol:chloroform 99:1


dx.doi.org/10.1021/ic4003548 | Inorg. Chem. 2013, 52, 5366–5377

(v/v) solution and on oleic acid capped $TiO_2$ in the same solvent.[14]

As told before, the average solvation relaxation time, $\langle\tau_s\rangle$, in water and in acetonitrile is reported to be ~500−600 fs. This eliminates the possibility of the 25 ps component arising due to solvation. The transient studies have been carried out by excitation at the blue edge of the MLCT band. This necessitates simultaneous electron localization in all three bipyridine ligands after initial photoexcitation. The 25 ps component is therefore tentatively assigned to interligand electron redistribution along the $^3$MLCT potential energy surface.[31] The lifetimes of the MLCT state of Ru(II)-polypyridyl complexes are known to be >100 ns,[32] so we can safely assume that it is the long lifetime of this state that is mirrored in the decay trace for **3** that does not decay until 400 ps.

The transient absorption spectrum of **4** (Figure 6) shows two bands at 540−720 and 760−1000 nm in addition to a negative

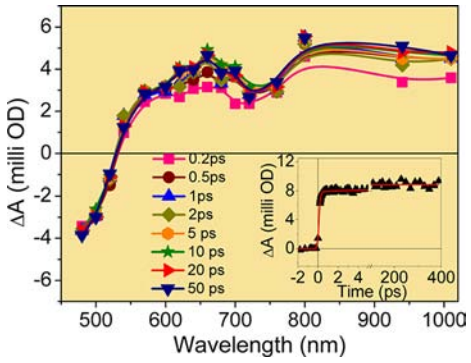


**Figure 6.** Transient absorption spectrum of **4** at different delay times in water:acetonitrile 99:1 (v/v) medium measured after 400 nm (fwhm <120 fs) excitation. Concentration of **4** is ~200 $\mu$M. Shown in the inset is the kinetic trace for **4** monitored at 900 nm.

absorption below 520 nm due to ground-state bleach. Following an argument similar to that in the case of **3**, these bands are assigned to excited triplet state absorption.[9b] An important point to note in the transient absorption spectrum is the absence of any bleach band in the 560−750 nm region, corresponding to the ground-state $^3$MLCT absorption. This is probably due to the higher molar extinction coefficient of the excited state relative to the aforesaid ground-state absorption so that the former dominates the transient absorption spectrum.

The kinetic trace monitored for **4** at 900 nm (Figure 6 inset) shows a 13 ps rise (10.2%) after initial population of the excited state (<120 fs, 89.8%). This 13 ps component is again assigned tentatively to interligand electron redistribution along the $^3$MLCT potential energy surface.[33]

The redox potential values could be obtained only for two bipyridine ligands in **3** and **4** from the electrochemical studies (vide supra). The most positive of these, that is, −1.39 V for **3** and −1.37 V for **4**, indisputably corresponds to the reduction of the coordinated ligand **2**.[6b] The other redox potential value is −1.52 V for **3**, that is, 0.13 V more negative. On the other hand, this difference is 0.21 V for **4** for which the second reduction appears at −1.58 V. This implies the fact that, as compared to **3**, for **4**, the $^3$MLCT potential energy surface corresponding to the ligand **2** is energetically more distantly placed than the other 2,2′-bipyridine ligands. Considering Marcus normal region behavior of interligand electron redistribution,[34] this presumably is the reason for which the aforesaid interligand electron redistribution occurs at a faster rate in **4** than in **3**.

Transient absorption spectrum of **3** on $TiO_2$ nanoparticle surface is shown in Figure 7a. The spectrum shows two major

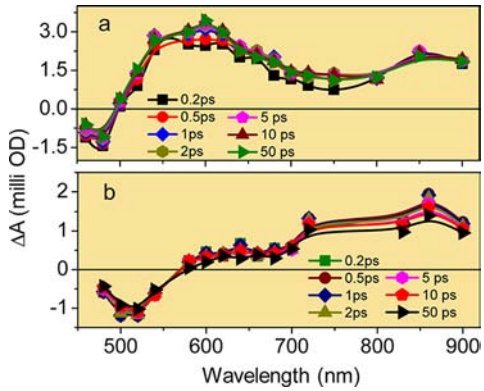


**Figure 7.** Transient absorption spectrum of (a) **3** and (b) **4** on $TiO_2$ (15 g/L) in water:acetonitrile 99:1 (v/v) medium at different delay times measured after 400 nm (fwhm <120 fs) excitation. Concentrations of **3** and **4** are ~100 $\mu$M.

absorption bands in the regions 500−700 and 760−900 nm. The former band can be irrefutably assigned to the formation of the cation radical ($\mathbf{3}^{\bullet+}$). Assignment of this band has been made on the basis of the results obtained in a complementary pulse radiolysis experiment where $\mathbf{3}^{\bullet+}$ has been generated selectively by the reaction of $N_3$ radical with **3** in $N_2O$-saturated aqueous solution (5% acetonitrile + 95% water) (Figure S3a, Supporting Information). This assignment is also corroborated by the previously reported transient absorption spectrum of **5** where the cation radical appears in the 500−670 nm region with the absorption peak at 590 nm.[6b] Numerous other studies on similar ruthenium polypyridyl complexes corroborate this assignment.[9a−c,e]

The lower energy absorption band in the 760−900 nm region can be assigned to electrons in the conduction band of $TiO_2$ nanoparticles. Again, this assignment is corroborated by previous literature reports where it has been shown that electrons in the conduction band can be detected by visible, near-IR, and mid-IR absorption.[3a,e,35] In addition to these bands, a negative absorption can be seen below 500 nm due to the ground-state bleach.[6b,9a,b,11] The transient absorption spectrum of **4** (Figure 7b) again presents two absorption bands between 560−680 and 720−900 nm. The first absorption band can again be assigned to the formation of cation radical ($\mathbf{4}^{\bullet+}$) based on our complementary pulse radiolysis experiment to generate $\mathbf{4}^{\bullet+}$ selectively as described above and also by previous results from our group on a similar osmium complex (Figure S3b, Supporting Information).[9b] The cation radical appears at 520−660 nm in this reported complex where there is no double bond between bipyridine and catechol. Apparently, the enhanced conjugation because of the presence of the double bond in **4** shifts the absorption band of the cation radical to higher wavelengths.

Before discussing the individual kinetics of **3** and **4** on $TiO_2$, a brief review of the kinetic data of the **5**−$TiO_2$ system is necessary. One of the biggest endeavors of the ultrafast spectroscopists working in the area of dye-sensitized solar cells worldwide is perhaps the maintenance of a steady and high electron concentration in the conduction band of $TiO_2$ after the


dx.doi.org/10.1021/ic4003548 | Inorg. Chem. 2013, 52, 5366−5377

elementary charge injection process. Studies done on the metal polypyridyl dyes with catecholate anchoring groups reveal two very important findings, the first being the fact that electron injection occurs single exponentially in less than 100 fs (this temporal resolution does not allow an accurate determination of the rate of electron injection process).[6b,9a−d,11] This corresponds to an electron injection rate of $>10^{13}$ $s^{-1}$, which has been explained in light of a very strong coupling of the dye and a large density of acceptor states in $TiO_2$ such that the electron transfer process falls in the so-called nonergodic limit.[7,8] Electron injection in the nonergodic regime is valuable in the sense that it ensures exploitation of the full energy of the incident photons by taking place before thermal electron relaxation and reorganization of the inner-sphere ligand environment. This nonergodicity, however, cannot be harvested in such systems because of the very deleterious BET reaction. The BET of the electrons to the oxidized ruthenium center involves a d orbital localized on the ruthenium metal whose electronic overlap with the $TiO_2$ conduction band is little and is further lessened by a spatial contraction of the wave function upon oxidation of Ru(II) to Ru(III).[36] As a result, the electronic coupling element for the BET reaction is 1 or 2 orders of magnitude smaller as compared to that for electron injection, reducing the back reaction rate by at least the same factor.[36] For **5** bound to $TiO_2$, even with this expected slowing, the BET rate is much faster as compared to the recovery of the ground state of the classical N3 dye, which occurs in microsecond−millisecond time scales.[3f,36] This makes this catechol dye incongruous for any sensible applications.

To slow this inherently fast BET, several approaches have been adopted by our research group, unfortunately not to much effect. The effects of secondary electron donating groups appended to the primary Ru(II) redox center are outcasted by the fast geminate charge recombination rates.[9e] A related study suggested that Ru(II)−polypyridyl complexes comprising of LLCT states can be a better photosensitizer in terms of improved electron injection yield and slow BET processes than complexes comprised of MLCT states.[11] However, the complicated synthetic procedure of these complexes places a question mark on their practical applicability. Another study from our group employed sequential energy and electron transfer in a catecholate bound Ru−Os−Ru cluster, and a slower BET rate could be obtained.[12] This slow BET rate was argued to be associated with the delocalization of the hole in the trinuclear complex radical cation. Nevertheless, for practical applications, such bulky molecules might present serious shortcomings in terms of not only synthetic viability but also photocurrent yields because of their lower surface coverage and probable tendency to aggregate. On the basis of this knowledge, we set out on the task of lowering the BET rates by a modification of the molecular skeleton itself, thus avoiding any cumbersome synthesis and exclusive of making the molecule any bulkier, and have developed a ruthenium(II)/osmium(II)/rhenium(I)-polypyridyl-based sensitizer system containing resorcinol instead of catechol as the enediol anchor. Our very recent work on the ultrafast interfacial electron transfer dynamics of the ruthenium(II)- and rhenium(I)-polypyridyl complexes on oleic acid capped $TiO_2$ in chloroform has indeed corroborated our hypothesis.[14]

An analysis of the kinetic traces of **3**−$TiO_2$ at various wavelengths presents the most striking results. The lower panel of Figure 8 shows a comparison of the normalized kinetic traces for the ground-state bleach recovery of the **3**−$TiO_2$ and **5**−$TiO_2$ systems both monitored at 480 nm.

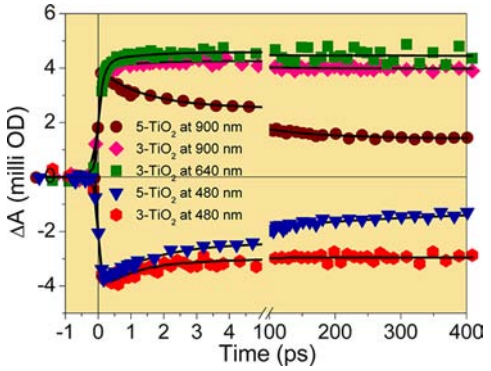


**Figure 8.** Comparison of the kinetic traces of **3** and **5** adsorbed on $TiO_2$ at 480 nm (lower panel) and comparison of the electron injection dynamics of the **3**−$TiO_2$ system with that of the **5**−$TiO_2$ system with the kinetic traces normalized with respect to the ultrafast growth component (upper panel).

The kinetic trace of **3**−$TiO_2$ at 480 nm can be fitted multiexponentially with $\tau_1$ < 120 fs (−100%), $\tau_2$ = 1.2 ps (+29%), $\tau_3$ = 33 ps (+1.3%), and $\tau_4$ > 400 ps (+69.7%) in contrast to the $\tau_1$ < 120 fs (−100%), $\tau_2$ = 1.5 ps (+37.6%), $\tau_3$ = 70 ps (+19.4%), and $\tau_4$ > 400 ps (+43%) fit of the kinetic trace for **5**−$TiO_2$ (Table 1). The ground-state bleach recovery represents the true geminate recombination dynamics and a look at the residuals at 400 ps suggests a not less than 30% slowing in this primary charge recombination rate, such a phenomenal effect having been brought about just by changing the position of the hydroxyl groups with respect to each other.

**Table 1. Lifetimes of the Transients for 3− and 5−$TiO_2$ Systems at Different Wavelengths**

| system | monitoring wavelength (nm) | lifetimes |
|---|---|---|
| **3**-$TiO_2$ | 480 | <120 fs (−100%), 1.2 ps (+29%), 33 ps (+1.3%), >400 ps (+69.7%) |
| | 640 | <120 fs (+89.5%), 1.5 ps (+10.5%), 33 ps (−3.1%), >400 ps (−96%) |
| | 900 | <120 fs (+92.5%), 1.5 ps (+7.5%), 33 ps (−65%), >400 ps (−92%) |
| **5**-T1$O_2$ | 480 | <120 fs (−100%), 1.5 ps (+37.6%), 70 ps (+19.4%), >400 ps (+43%) |
| | 900 | <120 fs (+100%), 1.5 ps (−34.8%), 70 ps (−26.8%), >400 ps (−38.4%) |

The electron injection time in the **3**−$TiO_2$ system is monitored by the time of appearance of the electron signal at 900 nm. Similar to that on oleic acid capped $TiO_2$ in chloroform,[14] electron injection is found to be fitting with $\tau_1$ < 120 fs (+92.5%) and $\tau_2$ = 1.5 ps (+7.5%) at 900 nm followed by a decay with time constants $\tau_3$ = 33 ps (−6.5%) and $\tau_4$ > 400 ps (−92%) (Figure 8, upper panel). This is in stark contrast to a < 120 fs only electron injection from the hot $^1$MLCT and/or $^3$MLCT states observed in case of the **5**−$TiO_2$ system which decays with $\tau_1$ = 1.5 ps (−34.8%), $\tau_2$ = 70 ps (−26.8%), and $\tau_3$ > 400 ps (−38.4%) time constants (Table 1). It may be noted that injection component in addition to the pulse width limited <120 fs component is a very rare observation for ruthenium polypyridyl enediol complexes as sensitizers.


dx.doi.org/10.1021/ic4003548 | Inorg. Chem. 2013, 52, 5366−5377

To comprehend the true origin of the 1.5 ps injection component in the kinetic trace of the electron signal, we recorded the kinetic trace for the decay of the cation radical signal at 640 nm (Figure 8, upper panel) and it is found to be fitting with $\tau_1$ < 120 fs (+89.5%), $\tau_2$ = 1.5 ps (+10.5%), $\tau_3$ = 33 ps (−3.1%), and $\tau_4$ > 400 ps (−96%). Again, two injection times are observed; however, the amplitude of the 1.5 ps component is greater than that observed in case of electron signal. The concerned difference, although small, represents a genuine difference in amplitudes, and, keeping in mind the extremely small noise (<0.1%) at these wavelengths, any fitting errors can be safely ruled out. While discussing the kinetic data for the free dye, we came across a 1 ps component that we assigned to a thermal electron relaxation to the thexi state. Thus, we can see that the 1.5 ps component observed in the kinetic traces of the conduction band electron signal and the cation radical signal corresponds to the component due to vibrational relaxation in the free dye dynamics and is therefore attributed to electron injection from the thermally relaxed $^3$MLCT states. That this component is indeed due to electron injection from the thermally relaxed states is proved by the fact that the relative amplitude of the component is greater in case of the cation radical signal where the probe pulse (at 640 nm) is of higher energy than that when the electron signal is being monitored (at 900 nm). The pulse width limited component, on the other hand, is attributed to electron injection from hot singlet/triplet Franck−Condon states as in the case for **5**−$TiO_2$. An interesting point to note is that the residuals at 400 ps for the cation radical in the **3**−$TiO_2$ system at 640 nm are no less than 96% as compared to a mere 38% for the **5**−$TiO_2$ system at the same time.

The electron injection rate from the dye to the semiconductor is determined by many factors, an important one of which is the potential energy difference between the dye excited state and conduction band edge.[3c,37] A higher excited state of the dye results in injection in a higher density of states, thus resulting in a very fast injection. For **5**, the $^3$MLCT state lies at −0.68 V, while for **3**, the same state lies at −0.91 V. With the $TiO_2$ conduction band edge at −0.5 V,[25] it is evident that in the **3**−$TiO_2$ system the electron injection rate should be faster. Instead, we observe a slower component. This clearly suggests that some other factor is being operational.

One of the other factors affecting the electron injection rate is the electronic coupling between the electron-donating orbital of the adsorbate and the electron-accepting orbital of the semiconductor.[3e,35c] Apparently, in both **3** and **5**, the $\pi^*$ orbital of the almost similarly substituted bipyridine is the electron-donating ligand overlapping with the $\pi$ symmetry $t_{2g}$ d orbital of $Ti^{4+}$ in $TiO_2$ However, the situation is somewhat more intricate.

Catechol is long known to interact with $TiO_2$ with the formation of a stable five-membered ring involving only one Ti atom of the whole nanocluster.[13] This is certainly much improbable of an interaction to occur in case of resorcinol where the hydroxyl groups are disposed further away from each other. Any reasonable interaction is therefore expected to involve at least more than one Ti atom. This proposition is proved by one of the recent works from our group where theoretical calculations have proved that the energy minimized structure for the molecule resorcinol binding to $TiO_2$ on the {101} anatase plane of a titanium dioxide cluster [$Ti_8O_{32}$] involves multiple nonadjacent Ti atoms.[38] This suggests a probably weaker overlap of the bipyridine $\pi^*$ orbital with the d orbital network of $TiO_2$ as compared to that in case of catechol. Formation constants have also been calculated to show that binding of resorcinol on $TiO_2$ is relatively weaker as compared to the binding of catechol.[38] We therefore believe that this comparatively weaker resorcinolate binding serves as the cause for the slower injection component in case of **3**−$TiO_2$ as compared to that in the **5**−$TiO_2$ system similar to that on oleic acid capped $TiO_2$ in chloroform.[14]

Furthermore, transient absorption studies carried out on the aforesaid resorcinol−$TiO_2$ system showed long time offset, which persisted with significant amplitudes up to >200 ps as compared to almost complete recombination for the molecule catechol binding to $TiO_2$.[38]

These observations tend to suggest that, as a result of increasing the number of Ti atoms and the Ti−Ti distance involved in the binding, not only is the electronic coupling ($H_{AB}$) reduced, but there is also a significant change in the electronic structure of the excited state involving the $\pi^*$ orbital of the bipyridine ligand and the $\pi$ symmetry $t_{2g}$ d orbital of $Ti^{4+}$ in $TiO_2$ as one moves from catechol to resorcinol. This change in the electronic structure of the excited state implies a much greater degree of charge delocalization as we move from catechol to resorcinol. In other words, as we move from catechol to resorcinol, because of the reduced electronic coupling and because of this enhanced charge diffusion along different directions into the bulk $TiO_2$, a significantly slower charge recombination rate in the kinetic traces of **3** on $TiO_2$ is observed. A similar observation on oleic acid capped $TiO_2$ in chloroform further corroborates this hypothesis.[14]

Following the Marcus semiclassical electron transfer theory, the BET rate can be expressed as a function of the driving force, reorganization energy, and the coupling element in the following way (eq 1):[39]

$$k_{BET} = \left(\frac{2\pi}{\hbar}\right)[H_{AB}]^2 \frac{1}{\sqrt{4\pi\Lambda kT}} \exp\left\{-\frac{(\Delta G^0 + \Lambda)^2}{4\Lambda kT}\right\} \quad (1)$$

Now, the charge recombination dynamics in a ruthenium polypyridyl dye−$TiO_2$ system falls in the Marcus inverted regime where with an increase in the thermodynamic driving force ($-\Delta G^0$), the BET rate decreases provided the coupling element remains the same (eq 1).[3i,9a,11,26,40] For the sake of argument, let us suppose that the coupling elements for **3**−$TiO_2$ and **5**−$TiO_2$ systems are indeed the same. Reorganization energy values are generally very small as compared to the driving force in the inverted region ($-\Delta G^0 \gg \lambda$, respective values for the classical N-719 dye being 1.5 and 0.3 eV);[36,38,40,41] the changes in the reorganization energy values, if any, will therefore be insignificant with respect to the changes in the driving force values. Now, $\Delta G^0$ is $E_C - E_{S/S+}$,[9a,e,42] where $E_C$ is the potential of the conduction band edge (−0.5 V)[25] and $E_{S/S+}$ is the ground-state redox potential of the dye, which is 1.25 V for **3** and 1.32 V for **5**. Using the above equation, the ($-\Delta G^0$) values for **3**−$TiO_2$ and **5**−$TiO_2$ systems are, respectively, calculated to be 1.75 and 1.82 eV. The recombination should therefore be faster for the **3**−$TiO_2$ system, which is contrary to what we observe. Thus, we see that the electron recombination rate cannot be explained on the basis of changes in free energy alone and that coupling plays a significant role.


dx.doi.org/10.1021/ic4003548 | Inorg. Chem. 2013, 52, 5366−5377

Logically, a similar reasoning, as thought of for explaining the injection dynamics of **3** on $TiO_2$, should apply in case of the **4**–$TiO_2$ system as well. To our surprise, this is not the case. Electron injection in both **4**–$TiO_2$ and **6**–$TiO_2$ systems is pulse width limited and is found to be fitting to <120 fs only, as monitored by the time of appearance of the conduction band electron signal. The kinetic trace for the decay of the signal in the **4**–$TiO_2$ system recorded at 620 nm can be fitted with 0.9 ps (−29.4%), 22 ps (−9.4%), and >400 ps (−61.2%) time constants (Figure S4, Supporting Information), while the decay of the conduction band electron signal at 900 nm can be fitted with 0.9 ps (−20.9%), 22 ps (−10.4%), and >400 ps (−68.7%) time constants (Figure 9 and Table 2). On the other hand, the

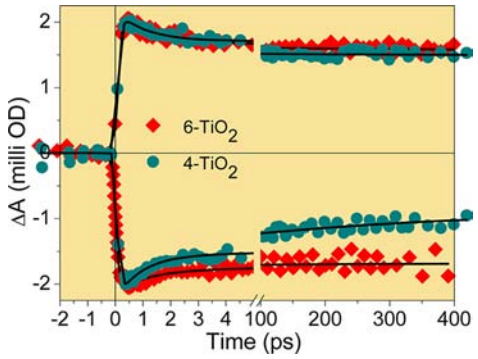


**Figure 9.** Comparison of the kinetic traces of **4** and **6** adsorbed on $TiO_2$ at 480 nm (lower panel) and 900 nm (upper panel).

**Table 2. Lifetimes of the Transients at Different Wavelengths for 4– and 6–$TiO_2$ Systems**

| system | monitoring wavelength (nm) | lifetimes |
|---|---|---|
| **4**–$TiO_2$ | 480 | <120 fs (−100%), 0.9 ps (+28.5%), 22 ps (+10.3%), >400 ps (+61.2%) |
| | 620 | <120 fs (+100%), 0.9 ps (−29.4%), 22 ps (−9.4%), >400 ps (−61.2%) |
| | 900 | <120 fs (+100%), 0.9 ps (−20.9%), 22 ps (−10.4%), >400 ps (−68.7%) |
| **6**–$TiO_2$ | 480 | <120 fs (−100%), 1.2 ps (+16.5%), 10 ps (+3.5%), >400 ps (+80%) |
| | 900 | <120 fs (+100%), 1.2 ps (−22.5%), 10 ps (−3.5%), >400 ps (−74%) |

decay of the conduction band electron signal for the **6**–$TiO_2$ system at 900 nm can be fitted with 1.2 ps (−22.5%), 10 ps (−3.5%), and >400 ps (−74%) time constants.

Lian and co-workers studied a series of ruthenium polypyridyl complexes, and they proved that in the non-adiabatic limit, provided coupling and reorganization energy parameters are the same, with an increase in the excited-state energies the electron injection rates become faster.[35c,43] They explained their observation by considering electron injection in successively higher density of states with successive increase in the excited-state energies of the sensitizer dyes. In our case, we observe that the $^3$MLCT excited state of **4** lies higher at −0.98 V as compared to that of **3** at −0.91 V (Scheme 4). Following an analogy similar to that of Lian et al., this means that for the **4**–$TiO_2$ system electron injection takes place in a relatively higher density of states as compared to that in the case of the **3**–$TiO_2$ system.

This, therefore, might be the reason for the absence of any slow component in the electron injection parameters, which supersedes the effects of weaker coupling of resorcinolate binding. Ultrafast <120 fs electron injection in the already reported rhenium(I)-polypyridyl resorcinol complex further corroborates this hypothesis.[14] The lower panel of Figure 9 compares the BET dynamics of **4**–$TiO_2$ and **6**–$TiO_2$ systems based on the recovery of the ground-state bleach monitored at 480 nm. The recovery in the **4**–$TiO_2$ system can be fitted with 0.9 ps (+28.5%), 22 ps (+10.3%), and >400 ps (+61.2%), while that in the **6**–$TiO_2$ system can be fitted with 1.2 ps (+16.5%), 10 ps (+3.5%), and >400 ps (+80%) (Table 2). The recombination dynamics in the **4**–$TiO_2$ system is therefore ∼20% faster than that in the **6**–$TiO_2$ system. This also is wholly contrary to that observed in case of the corresponding ruthenium complex **3** on $TiO_2$. The aforesaid trend is visible in the electron signal at 900 nm as well but is not prominent because of possible electron trapping at various trap sites of different trap energies and distances from the adsorbed dye.[44]

This faster recombination observed in case of the **4**–$TiO_2$ system can be explained again on the basis of Marcus theory. We have mentioned before that the charge recombination dynamics in such systems falls in the Marcus inverted regime where with an increase in the thermodynamic driving force ($-\Delta G^0$), the BET rate (given by eq 1) decreases provided coupling parameters are the same. Electron recombination in the case of the **3**–$TiO_2$ system is seen to be governed by the nature of electronic coupling of the dye to $TiO_2$ (vide supra). This factor therefore must apply in case of the **4**–$TiO_2$ system as well, and this would have governed the recombination rate provided the other factors were maintained the same, and this is not the case for the osmium complexes. The ($-\Delta G^0$) values for the **4**–$TiO_2$ and **6**–$TiO_2$ systems are calculated to be 1.3 and 1.64 eV, respectively. A significantly lower ($-\Delta G^0$) value (0.34 eV) in the **4**–$TiO_2$ system, which again presides over the electronic coupling effects, presumably results in the faster recombination observed. In case of the ruthenium complexes, this difference in the ($-\Delta G^0$) values between the catecholate and resorcinolate binding analogues is only 0.07 eV, which, we believe, is not enough to outdo the effects of resorcinolate binding.

## 4. CONCLUSION

Femtosecond transient absorption studies with our newly synthesized sensitizer dyes reinforce the fact that by replacing catechol-based enediol anchoring groups with those based on resorcinol, that is, by merely changing the position of the hydroxyl groups, the exceedingly deleterious geminate charge recombination in ruthenium polypyridyl enediol-based sensitizers can be slowed outstandingly. This substitute anchoring group, as a result of its weak binding with $TiO_2$ and similar to that on oleic acid capped $TiO_2$ in chloroform, elicits electron injection simultaneously from the thermalized $^3$MLCT states in addition to the sub 100 fs electron injection from the hot singlet/triplet MLCT states. This study therefore strengthens our assertion of resorcinol to be a very promising anchoring group toward the development of efficient sensitizers for use in dye-sensitized solar cells. Studies on the efficiency and the current voltage characteristics of such dyes are currently underway in our laboratory. A point, however, to be taken care of while designing the dyes is that the ground-state redox level of the dye must not be too cathodic to prevent possible inverted region effects presiding over effects of weak binding, as


dx.doi.org/10.1021/ic4003548 | Inorg. Chem. 2013, 52, 5366–5377

**Scheme 4. Mechanistic Scheme Showing the Different Electron Transfer Processes in 3, 4, 5, and 6 Adsorbed on $TiO_2$**

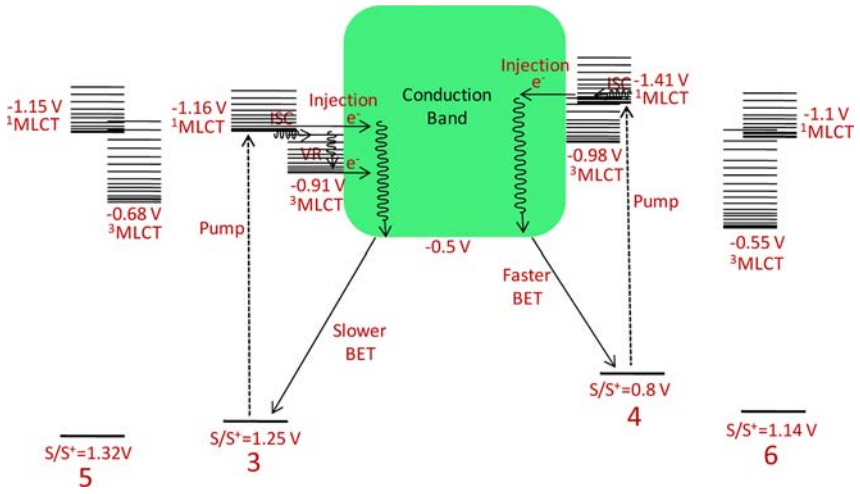


is evident from a study of the BET rate of the corresponding Os(II)-polypyridyl dye.

## ■ ASSOCIATED CONTENT

### Ⓢ Supporting Information

Transient absorption spectrum of the cation radical of **3** and **4** obtained from one electron pulse radiolysis, kinetic trace for the decay of the cation radical in the **4**–$TiO_2$ system, SAED pattern of $TiO_2$ nanoparticles, and comparison of the absorptance and the excitation spectra of **3** and **4**. This material is available free of charge via the Internet at http://pubs.acs.org.

## ■ AUTHOR INFORMATION

### Corresponding Author

*Fax: (+) 91-22-25505331/25505151 (H.N.G.); 00-91-278-2567562 (A.D.). E-mail: hnghosh@barc.gov.in (H.N.G.); amitava@csmcri.org (A.D.).

### Notes

The authors declare no competing financial interest.

## ■ ACKNOWLEDGMENTS

We thank Dr. D. K. Palit, Dr. S. K. Sarkar, and Dr. T. Mukherjee of Bhabha Atomic Research Centre of Mumbai and Dr. P. K. Ghosh of Central Salt & Marine Chemicals Research Institute (CSIR), Bhavnagar, for their encouragement and continuous support. A.D. and H.N.G. acknowledge BRNS for financial support. A.D. also thanks MNRE/CSIR for funds through CSIR TAP-SUN Programme. T.B. acknowledges BRNS & CSIR for research fellowship. We also thank Analytical Discipline and Centralized Instrument Facilities, CSMCRI, for assistance with different analytical and spectroscopic measurements.

## ■ REFERENCES

(1) (a) Durrant, J. R.; Haque, S. A.; Palomares, E. *Coord. Chem. Rev.* **2004**, *248*, 1247. (b) Schwarzburg, K.; Ernstorfer, R.; Felber, S.; Willig, F. *Coord. Chem. Rev.* **2004**, *248*, 1259. (c) Hagfeldt, A.; Grätzel, M. *Acc. Chem. Res.* **2000**, *33*, 269. (d) Peter, L. *Acc. Chem. Res.* **2009**, *42*, 1839. (e) Anderson, N. A.; Lian, T. *Annu. Rev. Phys. Chem.* **2005**, *6*, 491. (f) Anderson, N. A.; Lian, T. *Coord. Chem. Rev.* **2004**, *248*, 1231. (g) Brennaman, M. K.; Patrocinio, A. O. T.; Song, W.; Jurss, J. W.; Concepcion, J. J.; Hoertz, P. G.; Traub, M. C.; Iha, N. Y. M.; Meyer, T. J. *ChemSusChem* **2010**, *4*, 216. (h) Song, W.; Brennaman, M. K.; Concepcion, J. J.; Jurss, J. W.; Hoertz, P. G.; Luo, H.; Chen, C.; Kenneth, H. G.; Meyer, T. J. *J. Phys. Chem. C* **2011**, *115*, 7081. (i) More references of the works from the Solar Fuels EFRC centered at UNC, Chapel Hill, on the use of dye-sensitized architectures for aqueous photoelectrochemical fuel-forming applications can be found at http://www.efrc.unc.edu/.

(2) (a) Ardo, S.; Meyer, G. J. *Chem. Soc. Rev.* **2009**, *38*, 115. (b) Abrahamsson, M.; Johansson, P. G.; Ardo, S.; Kopecky, A.; Galoppini, E.; Meyer, G. J. *J. Phys. Chem. Lett.* **2010**, *1*, 1725. (c) Guo, J.; She, C.; Lian, T. *J. Phys. Chem. C* **2007**, *111*, 8979. (d) Clifford, J. N.; Palomares, E.; Nazeeruddin, M. K.; Grätzel, M.; Durrant, J. R. *J. Phys. Chem. C* **2007**, *111*, 6561. (e) Maggio, E.; Martsinovich, N.; Troisi, A. *J. Phys. Chem. C* **2012**, *116*, 7638. (f) Barzykin, A. V.; Tachiya, M. *J. Phys. Chem. B* **2002**, *106*, 4356. (g) Kallioinen, J.; Benko, G.; Sundstrom, V.; Korppi-Tommola, J. E. I.; Yartsev, A. P. *J. Phys. Chem. B* **2002**, *106*, 4396. (h) Kuciauskas, D.; Monat, J. E.; Villahermosa, R.; Gray, H. B.; Lewis, N. S.; McCusker, J. K. *J. Phys. Chem. B* **2002**, *106*, 9347. (i) Palomares, E.; Martinez-Diaz, M. V.; Haque, S. A.; Torres, T.; Durrant, J. R. *Chem. Commun.* **2004**, 2112. (j) McFarland, S. A.; Lee, F. S.; Cheng, K. H. W. Y.; Cozens, F. L.; Schepp, N. P. *J. Am. Chem. Soc.* **2005**, *127*, 7065.

(3) (a) Hannappel, T.; Burfeindt, B.; Storck, W.; Willig, F. *J. Phys. Chem. B* **1997**, *101*, 6799. (b) She, C.; Guo, J.; Irle, S.; Morokuma, K.; Mohler, D. L.; Zabri, H.; Odobel, F.; Youm, K.-T.; Liu, F.; Hupp, J. T.; Lian, T. *J. Phys. Chem. A* **2007**, *111*, 6832. (c) Chen, Y.-S.; Li, C.; Zeng, Z.-H.; Wang, W.-B.; Wang, X.-S.; Zhang, B.-W. *J. Mater. Chem.* **2005**, *15*, 1654. (d) Tachibana, Y.; Haque, S. A.; Mercer, I. P.; Durrant, J. R.; Klug, D. R. *J. Phys. Chem. B* **2000**, *104*, 1198. (e) Asbury, J. B.; Ellingson, R. J.; Ghosh, H. N.; Ferrere, S.; Nozik, A. J.; Lian, T. *J. Phys. Chem. B* **1999**, *103*, 3110. (f) Tachibana, Y.; Moser, J. E.; Grätzel, M.; Klug, D. R.; Durrant, J. R. *J. Phys. Chem.* **1996**, *100*, 20056. (g) Argazzi, R.; Bignozzi, C. A.; Heimer, T. A.; Castellano, F. N.; Meyer, G. J. *J. Am. Chem. Soc.* **1995**, *117*, 11815. (h) Heimer, T. A.; D'Arcangelis, S. T.; Farzad, F.; Stipkala, J. M.; Meyer, G. J. *Inorg. Chem.* **1996**, *35*, 5319. (i) Bonhote, P.; Moser, J. E.; Vlachopoulos, N.; Walder, L.; Zakeeruddin, S. M.; Humphry-Baker, R.; Pechy, P.; Grätzel, M. *Chem. Commun.* **1996**, 1163. (j) McNamara, W. R.; Snoeberger, R. C., III; Li, G.; Schleicher, J. M.; Cady, W. C.; Poyatos, M.; Schmuttenmaer, C. A.; Crabtree, R. H.; Brudvig, G. W.; Batista, V. S. *J. Am. Chem. Soc.* **2008**, *130*, 14329.

(4) (a) Nazeeruddin, M. K.; Zakeeruddin, S. M.; Humphry-Baker, R.; Jirousek, M.; Liska, P.; Vlachopoulos, N.; Shklover, V.; Fischer, C. H.; Grätzel, M. *Inorg. Chem.* **1999**, *38*, 6298. (b) Montalti, M.; Wadhwa, S.; Kim, W. Y.; Kipp, R. A.; Schmehl, R. H. *Inorg. Chem.* **2000**, *39*, 76.

(5) Kalyansundaram, K.; Grätzel, M. *Coord. Chem. Rev.* **1998**, *77*, 347.

(6) (a) Rice, C. R.; Ward, M. D.; Nazeeruddin, M. K.; Grätzel, M. *New J. Chem.* **2000**, *24*, 651. (b) Ramakrishna, G.; Jose, D. A.; Krishna

Kumar, D.; Das, A.; Palit, D. K.; Ghosh, H. N. *J. Phys. Chem. B* **2005**, *109*, 15445.
(7) (a) Bernstein, R. B.; Zewail, A. H. *J. Phys. Chem.* **1986**, *90*, 3467. (b) Diau, E. W.-G.; Herek, J. L.; Kim, Z. H.; Zewail, A. H. *Science* **1998**, *279*, 847.
(8) (a) Benko, G.; Kallioinen, J.; Korppi-Tommola, J. E. I.; Yartsev, A. P.; Sundstrom, V. *J. Am. Chem. Soc.* **2002**, *124*, 489. (b) Hoertz, P. G.; Staniszewski, A.; Marton, A.; Higgins, g. T.; Incarvito, C. D.; Rheingold, A. L.; Meyer, G. J. *J. Am. Chem. Soc.* **2006**, *128*, 8234.
(9) (a) Kar, P.; Verma, S.; Das, A.; Ghosh, H. N. *J. Phys. Chem. C* **2009**, *113*, 7970. (b) Verma, S.; Kar, P.; Das, A.; Palit, D. K.; Ghosh, H. N. *Chem.-Eur. J.* **2010**, *16*, 611. (c) Kar, P.; Verma, S.; Sen, A.; Das, A.; Ganguly, B.; Ghosh, H. N. *Inorg. Chem.* **2010**, *49*, 4167. (d) Kar, P.; Banerjee, T.; Verma, S.; Sen, A.; Das, A.; Ganguly, B.; Ghosh, H. N. *Phys. Chem. Chem. Phys.* **2012**, *14*, 8192. (e) Banerjee, T.; Rawalekar, S.; Das, A.; Ghosh, H. N. *Eur. J. Inorg. Chem.* **2011**, 4187.
(10) (a) Agrazzi, R.; Bignozzi, C. A.; Heimer, T. A.; Castellano, F. N.; Meyer, G. M. *J. Phys. Chem. B* **1997**, *101*, 2591. (b) Bonhote, P.; Moser, J. E.; Humphrey-Baker, R.; Vlachopoulos, N.; Zakeeruddin, S. M.; Walder, L.; Grätzel, M. *J. Am. Chem. Soc.* **1999**, *121*, 1324. (c) Argazzi, R.; Bignozzi, C. A.; Heimer, T. A.; Castellano, F. N.; Meyer, G. J. *J. Am. Chem. Soc.* **1995**, *117*, 11815. (d) Xu, Y.; Sun, S.; Fan, J.; Peng, X. *J. Photochem. Photobiol., A: Chem.* **2007**, *188*, 317. (e) Pan, J.; Xu, Y.; Benko, G.; Feyziyev, Y.; Styring, S.; Sun, L.; Akermark, B.; Polivka, T.; Sundstrom, V. *J. Phys. Chem. B* **2004**, *108*, 12904. (f) Handa, S.; Wietasch, H.; Thelakkat, M.; Durrant, J. R.; Haque, S. A. *Chem. Commun.* **2007**, 1725. (g) Karthikeyan, C. S.; Wietasch, H.; Thelakkat, M. *Adv. Mater.* **2007**, *19*, 1091. (h) Haque, S. A.; Handa, S.; Peter, K.; Palomares, E.; Thelakkat, M.; Durrant, J. R. *Angew. Chem., Int. Ed.* **2005**, *44*, 5740.
(11) Verma, S.; Kar, P.; Das, A.; Ghosh, H. N. *Chem.-Eur. J.* **2011**, *17*, 1561.
(12) Verma, S.; Kar, P.; Banerjee, T.; Das, A.; Ghosh, H. N. *J. Phys. Chem. Lett.* **2012**, *3*, 1543.
(13) (a) Moser, J.; Punchihewa, S.; Infelta, P. P.; Grätzel, M. *Langmuir* **1991**, *7*, 3012. (b) Redfern, P. C.; Zapol, P.; Curtiss, L. A.; Rajh, T.; Thurnauer, M. C. *J. Phys. Chem. B* **2003**, *107*, 11419. (c) Duncan, W. R.; Prezhdo, O. V. *J. Phys. Chem. B* **2005**, *109*, 365. (d) Wang, Y.; Hang, K.; Anderson, N. A.; Lian, T. *J. Phys. Chem. B* **2003**, *107*, 9434. (e) Rajh, T.; Chen, L. X.; Lukas, K.; Liu, T.; Thurnauer, M. C.; Tiede, D. M. *J. Phys. Chem. B* **2002**, *106*, 10543.
(14) Banerjee, T.; Kaniyankandy, S.; Das, A.; Ghosh, H. N. *J. Phys. Chem. C* **2013**, *117*, 3084.
(15) Sullivan, B. P.; Salmon, D. J.; Meyer, T. J. *Inorg. Chem.* **1978**, *17*, 3334.
(16) Kober, E. M.; Caspar, J. V.; Sullivan, B. P.; Meyer, T. J. *Inorg. Chem.* **1988**, *27*, 4587.
(17) Verma, S.; Kar, P.; Das, A.; Palit, D. K.; Ghosh, H. N. *J. Phys. Chem. C* **2008**, *112*, 2918.
(18) (a) Nazeeruddin, M. K.; Zakeeruddin, S. M.; Kalyanasundaram, K. *J. Phys. Chem.* **1993**, *97*, 9607. (b) Pavlishchuk, V. V.; Addison, A. W. *Inorg. Chim. Acta* **2000**, *298*, 97.
(19) Kaniyankandy, S.; Rawalekar, S.; Verma, S.; Palit, D. K.; Ghosh, H. N. *Phys. Chem. Chem. Phys.* **2010**, *12*, 4210.
(20) Ghosh, H. N. *J. Phys. Chem. B* **1999**, *103*, 10382.
(21) Matylitsky, V. V.; Lenz, M. O.; Wachtveitl, J. *J. Phys. Chem. B* **2006**, *110*, 8372.
(22) (a) Jose, D. A.; Kar, P.; Koley, D.; Ganguly, B.; Thiel, W.; Ghosh, H. N.; Das, A. *Inorg. Chem.* **2007**, *46*, 5576. (b) Kalyanasundaram, K. *Photochemistry of Polypyridine and Porphyrin Complexes*; Academic Press: London, 1992; Chapter 6.
(23) (a) Estacio, S. G.; do Couto, P. C.; Cabral, B. J. C.; da Piedade, M. E. M.; Simoes, J. A. M. *J. Phys. Chem. A* **2004**, *108*, 10834. (b) Zaleta, B. G.; Balderas, R. G.; Trujillo, J. H. *Phys. Chem. Chem. Phys.* **2010**, *12*, 4783. (c) Pimentel, G. C.; McClellan, A. L. *The Hydrogen Bond*; W. H. Freeman: San Francisco, CA, 1960.
(24) Kuang, D.; Wenger, B.; Klein, C.; Moser, J. E.; Baker, R. H.; Zakeeruddin, S. M.; Grätzel, M. *J. Am. Chem. Soc.* **2006**, *128*, 4146.
(25) (a) Ramakrishna, G.; Ghosh, H. N. *J. Phys. Chem. A* **2002**, *106*, 2545. (b) Duonghong, D.; Ramsden, J.; Grätzel, M. *J. Am. Chem. Soc.* **1982**, *104*, 2917.
(26) Kaniyankandy, S.; Verma, S.; Mondal, J. A.; Palit, D. K.; Ghosh, H. N. *J. Phys. Chem. C* **2009**, *113*, 3593.
(27) Cannizo, A.; Mourik, F. V.; Gawelda, W.; Zgrablic, G.; Bressler, C.; Chergui, M. *Angew. Chem.* **2006**, *118*, 3246; *Angew. Chem., Int. Ed.* **2006**, *45*, 3174.
(28) Damrauer, N. H.; McCusker, J. K. *J. Phys. Chem. A* **1999**, *103*, 8440.
(29) Damrauer, N. H.; Cerullo, G.; Yeh, A.; Boussie, T. R.; Shank, C. V.; McCusker, J. K. *Science* **1997**, *275*, 54.
(30) (a) Jarzeba, W.; Walker, G. C.; Johnson, A. E.; Barbara, P. F. *Chem. Phys.* **1991**, *152*, 57. (b) Ramakrishna, G.; Jose, D. A.; Kumar, D. K.; Das, A.; Palit, D. K.; Ghosh, H. N. *J. Phys. Chem. B* **2006**, *110*, 10197.
(31) (a) Malone, R. A.; Kelley, D. F. *J. Chem. Phys.* **1991**, *95*, 8970. (b) Henrich, J. D.; Zhang, H.; Dutta, P. K.; Kohler, B. *J. Phys. Chem. B* **2010**, *114*, 14679 and references therein.
(32) Vlcek, A., Jr. *Coord. Chem. Rev.* **2000**, *200*, 933.
(33) Shaw, G. B.; Brown, C. L.; Papanikolas, J. M. *J. Phys. Chem. A* **2002**, *106*, 1483.
(34) Liard, D. J.; Vlcek, A., Jr. *Inorg. Chem.* **2000**, *39*, 485.
(35) (a) Zhang, J. Z. *Acc. Chem. Res.* **1997**, *30*, 423. (b) Colombo, D. P., Jr.; Bowman, R. M. *J. Phys. Chem.* **1996**, *100*, 18445. (c) Asbury, J. B.; Hao, E.; Wang, Y.; Ghosh, H. N.; Lian, T. *J. Phys. Chem. B* **2001**, *105*, 4545.
(36) Grätzel, M. *Inorg. Chem.* **2005**, *44*, 6841.
(37) Gerischer, H. Semiconductor Electrochemistry. In *Physical Chemistry: An Advance Treatise*; Eyring, H., Henderson, D., Jost, W., Eds.; Academic Press: New York, 1970; Vol. *9A*, p 463.
(38) Kaniyankandy, S.; Rawalekar, S.; Sen, A.; Ganguly, B.; Ghosh, H. N. *J. Phys. Chem. C* **2012**, *116*, 98.
(39) (a) Marcus, R. A. *Annu. Rev. Phys. Chem.* **1964**, *15*, 155. (b) Marcus, R. A.; Sutin, N. *Biochim. Biophys. Acta* **1985**, *811*, 265.
(40) (a) Meyer, G. J. *Inorg. Chem.* **2005**, *44*, 6852. (b) Clifford, J. N.; Palomares, E.; Nazeeruddin, M. K.; Grätzel, M.; Nelson, J.; Li, X.; Long, N. J.; Durrant, J. R. *J. Am. Chem. Soc.* **2004**, *126*, 5225. (c) Hagfeldt, A.; Grätzel, M. *Chem. Rev.* **1995**, *95*, 49. (d) Nakade, S.; Kanzaki, T.; Kubo, W.; Kitamura, T.; Wada, Y.; Yanagida, S. *J. Phys. Chem. B* **2005**, *109*, 3480. (e) Yan, S. G.; Hupp, J. T. *J. Phys. Chem.* **1996**, *100*, 6867.
(41) (a) Moser, J. E.; Grätzel, M. *Chem. Phys.* **1993**, *176*, 493. (b) Odobel, F.; Blart, E.; Lagree, M.; Villieras, M.; Boujtita, H.; Murr, N. E.; Caramoric, S.; Bignozzi, C. A. *J. Mater. Chem.* **2003**, *13*, 502. (c) Yang, M.; Thompson, D. W.; Meyer, G. J. *Inorg. Chem.* **2002**, *41*, 1254. (d) Hilgendorff, M.; Sundstrom, V. *J. Phys. Chem. B* **1998**, *102*, 10505. (e) Martini, I.; Hodak, J. H.; Hartland, G. V. *J. Phys. Chem. B* **1998**, *102*, 9508.
(42) Ramakrishna, G.; Das, A.; Ghosh, H. N. *Langmuir* **2004**, *20*, 1430.
(43) Asbury, J. B.; Anderson, N. A.; Hao, E.; Ai, X.; Lian, T. *J. Phys. Chem. B* **2003**, *107*, 7376.
(44) (a) Ramakrishna, G.; Singh, A. K.; Palit, D. K.; Ghosh, H. N. *J. Phys. Chem. B* **2004**, *108*, 4775. (b) Takeshita, K.; Sasaki, Y.; Kobashi, M.; Tanaka, Y.; Maeda, S.; Yamakata, A.; Ishibashi, T.; Onishi, H. *J. Phys. Chem. B* **2004**, *108*, 2963 and references therein.